

# Blood Flow in the Abdominal Aorta Post 'Chimney' Endovascular Aneurysm Repair

Hila Ben Gur<sup>1</sup> Moshe Halak<sup>2</sup> Moshe Brand<sup>3</sup>

<sup>1</sup>School of Mechanical Engineering Faculty of Engineering, Tel Aviv University Tel Aviv, Israel,  
hilabengur@mail.tau.ac.il

<sup>2</sup>Department of Vascular Surgery, The Chaim Sheba Medical Center, Tel Hashomer, Israel  
moshe.halak@sheba.health.gov.il

<sup>3</sup>Department of Mechanical Engineering and Mechatronics, Faculty of Engineering, Ariel University, Ariel, Israel  
mosheb@ariel.ac.il

## Abstract

Aortic aneurysms are a main death cause in the elderly population throughout the western world. In recent years, more aneurysm repairs are performed endovascularly using stent grafts (SGs) inserted into the aneurysm site through the arterial system (minimally invasive). In this study, we analyze the hemodynamics in an aneurysmatic abdominal aorta (AAA) endovascularly repaired by a stent graft (SG) system using the chimney technique. Computational fluid dynamics (CFD) is employed to study models of a healthy aorta versus an aorta post 'chimney' endovascular aneurysm repair (ChEVAR) using chimney stent grafts (CSG) inserted into each renal artery in parallel to the aortic SG. Results demonstrate that the presence of the CSGs results in stagnation regions and wall shear stress (WSS) modifications, yet the flow regime remains laminar. Thus, indicating the spatially contained effects of the ChEVAR technique and further supporting its merit.

*Keywords:* ChEVAR, abdominal aortic aneurysm (AAA), chimney stent grafts (CSG), computational fluid dynamics (CFD), hemodynamics, wall shear stresses (WSS)

## 1 Introduction

Aortic aneurysms are a main cause of death in the elderly population throughout the western world. The most common location for an aortic aneurysm formation is the infrarenal aorta (Guo *et al.*, 2006). The traditional and most prevailing method of aneurysm repair is open surgery, whereby a large incision in the patient's abdomen allows access to the aneurysm site.

In recent years, more aneurysm repairs are performed endovascularly, excluding the aneurysm sac using stent grafts (SGs) inserted into the aneurysm site through the arterial system (minimally invasive). Typically, small incisions in the groin are created in order to deliver the SG system to the repair site using the femoral arteries as entry points. Following SG implantation, the aneurysm sac is sealed and blood subsequently flows through the

newly created artificial conduit replacing the bulging part of the aorta.

A successful endovascular repair depends on the blood vessels and aneurysm morphologies. An aneurysm characterized by close proximity to a visceral artery ostium, is very challenging for endovascular repair. The requirement to properly seal the aneurysm sac while avoiding coverage of aortic branches by the SG can be very demanding. Innovative solutions for this type of problem include the fenestrated SG system. Fenestrated SGs are tailored to a specific patient morphology (Kandail *et al.*, 2014).

In urgent cases, where the patient cannot wait several months for a custom SG system to be fabricated, an innovative solution is recently being employed using off-the-shelf SGs. This solution involves an endovascular surgical procedure called the 'chimney' technique whereby parallel to the main aortic SG that excludes the aneurysm sac, one or more tubular covered stents ('chimneys') are inserted into the visceral arteries. These covered stents facilitate proper blood flow to arteries that would otherwise be blocked by the main aortic SG due to their proximity to the aneurysm sac. A common case of aneurysm repair using the 'chimney' technique is the two renal arteries being highly adjacent to the aneurysm (Figure 1). Thus, requiring a chimney stent graft (CSG) in each renal artery to preserve blood flow to the kidneys.

In this study, a healthy abdominal aorta was evaluated in comparison with several configurations of post ChEVAR aorta having CSG inserted into each renal artery (Figures 1 and 2).

Computational fluid dynamics (CFD, ANSYS Fluent package) simulations of pulsatile blood flow during the cardiac cycle were employed. An idealized anatomy of the abdominal aorta was modeled based on averages of measurements taken from cadaver specimens and patient angiograms (Moore *et al.*, 1992).

The effect of CSGs on abdominal aortic blood flow and wall shear stresses (WSS) was analyzed by examining blood flow patterns and regimes.

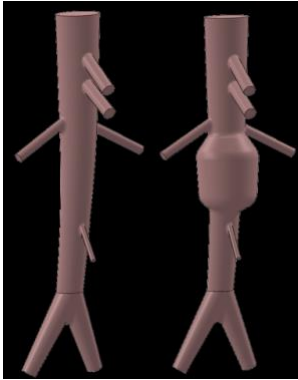


**Figure 1:** Left, healthy abdominal aorta model. Right, aneurysmatic aorta (aneurysm is adjacent to the renal branches).

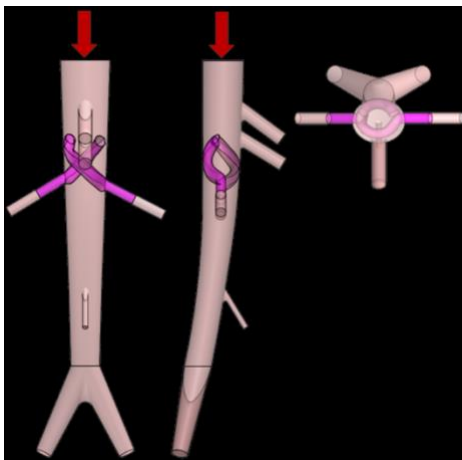


**Figure 2:** 3D model of the post ChEVAR abdominal aorta for analysis (aneurysm replaced by SG). Left to right: Front, side and top views, respectively. Red arrows: direction of blood flow.

## 2 Methodology

### 2.1 Governing Equations

The governing equations for blood flow in the abdominal aorta are the Navier Stokes momentum equations and the continuity equation for an incompressible fluid:

$$\rho \partial V / \partial t + \rho (V \cdot \nabla) V - \mu \Delta V + \nabla p = 0 \quad (1)$$

$$\nabla \cdot V = 0 \quad (2)$$

where  $v$ ,  $\rho$ ,  $\mu$  &  $p$  are the fluid velocity, density, dynamic viscosity the pressure field experienced by the fluid, respectively. Blood is not a Newtonian fluid – viscosity depends on the strain rate according to the Carreau model for shear thinning fluids:

$$\mu(\dot{\gamma}) = \mu_{\infty} + (\mu_0 - \mu_{\infty})(1 + \lambda^2 \dot{\gamma}^2)^{0.5(n-1)} \quad (3)$$

where  $\dot{\gamma}$  is the scalar flow shear rate and  $\mu_{\infty}$  &  $\mu_0$  are the viscosities for an infinitely large and zero strain rate, respectively.  $\lambda$  and  $n$  are fluid specific time constant and power behavior index. Blood density is assumed  $1045 \text{ kg/m}^3$  (Ene-Iordache *et al*, 2001).

### 2.2 Anatomical Model

The geometric 3D model employed for analyzing the idealized healthy abdominal aorta is presented in Figure 1. The model is based on angiograms and pressurized cadaver specimens measurements (Moore *et al*, 1992). The model incorporates the elliptical cross section, the tapering nature of the abdominal aorta, the arterial branches and the slight curvature towards the posterior wall. The model of the abdominal aorta post ChEVAR is based on the healthy model. Modifications were made in the model in order to account for the CSGs. The bulging part of the abdominal aorta is assumed completely replaced by the aortic SG, and thus is not a part of the numerical domain. The CSGs are modeled as long fabric-covered stents having a free diameter of 7 mm and a wall thickness of 0.1 mm, in compliance with suitable endograft dimensions often utilized in chimney repairs. The CSG models incorporate their helical-like nature (Coscas *et al*, 2011). A slightly flattened CSG region spanning from the orifice of the renal artery to the final contact region between the chimney and the aortic SG morphing the CSG cross section from a circle to an ellipse was also incorporated (de Bruin *et al*, 2013).

The CSGs protrude upstream into the aorta 10 mm above the main SG to avoid blockage of blood flow into the renal arteries.

### 2.3 Numerical Model

Blood flow behavior in the abdominal aorta during the cardiac cycle is considered to be predominantly laminar (Morris *et al*, 2004). Thus, a laminar CFD solver is employed. Literature demonstrates flow parameters e.g. WSS differ by as much as 30% between distensible and rigid blood vessel models (Shipkowitz *et al*, 1998). However, overall flow dynamics remain similar (Friedman *et al*, 1992). Thus, rigid wall approximation is sufficient for a comparative study.

No slip/penetration boundary conditions are applied at the walls. The inlet boundary condition employed is a pulsatile velocity function adapted from the literature - Figure 3 (Taylor *et al*, 1998). This waveform is decomposed into a Fourier series and modified to comply with the average velocity (flow rate). A parabolic profile distributed over the elliptical inlet is assumed (Shipkowitz *et al*, 1998). The domain has seven outlets with a constant flow ratio between them during the cardiac cycle (Moore *et al*, 1992). ANSYS Fluent CFD package (second order approximations) is used for the analysis.

### 2.4 Numerical Discretization

The model of the post ChEVAR abdominal aorta was meshed using 1.1 million polyhedral cells with 4 million nodes. The cycle time was discretized into 800 time steps. The scaled residuals value used was  $5 \cdot 10^{-6}$ . The numerical parameters used for the healthy aorta model were similar.

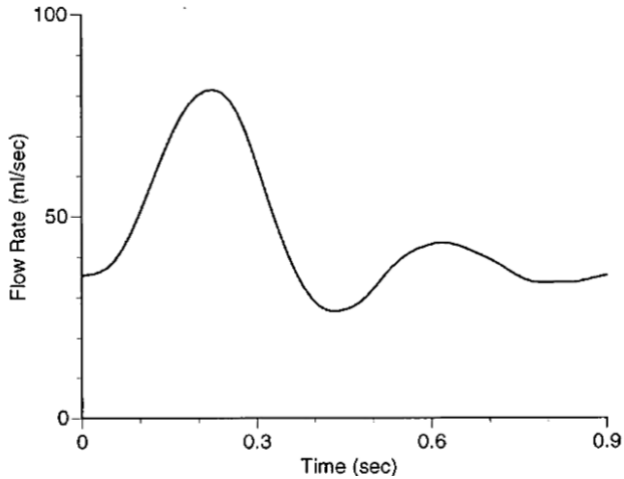


Figure 3: Waveform of the inlet flow rate [10].

## 3 Results

### 3.1 Validation

WSS for the healthy aorta (supra-celiac height) were compared with values measured in an experimental study (Moore *et al*, 1994).

WSSs were derived by extracting the temporal (during an entire cardiac cycle) minimum, maximum and average WSS values for each element of the supra-celiac ring of Figure 4. A spatial average of each parameter along the ring circumference was employed. Pulse WSS is defined as the difference between the maximum and minimum WSS for each element spatially averaged along the ring.

Results of this comparison are listed in Table 1 (Y/axial component). The relative errors indicate numerical results are in reasonable agreement with experimental data.

### 3.2 Flow Patterns

Stagnant regions are formed in the post ChEVAR aorta downstream near the CSGs. These regions persist throughout the cardiac cycle (Figures 5 and 6). There are no stagnant regions in the healthy model (Figures 7 and 8).

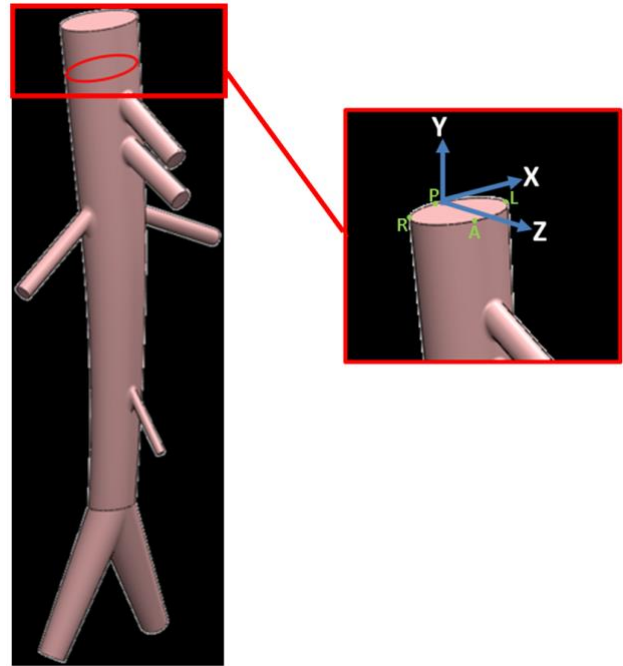


Figure 4: Left: WSS supra-celiac comparison surface (ring in red). Right: Coordinate system and sectors of a horizontal ring of the abdominal aorta wall. A - anterior sector, P - posterior sector, R - right sector, L - left sector.

Table 1. Numerical validation results for wss values (y/axial component) in the supra-celiac region.

	Minimum WSS [Pa]	Maximum WSS [Pa]	Average WSS [Pa]	Pulse WSS [Pa]
Numerical Model	-0.48	0.99	0.19	1.47
Experiment	-0.45	0.87	0.13	1.32
Relative Error [%]	6	14	44	12

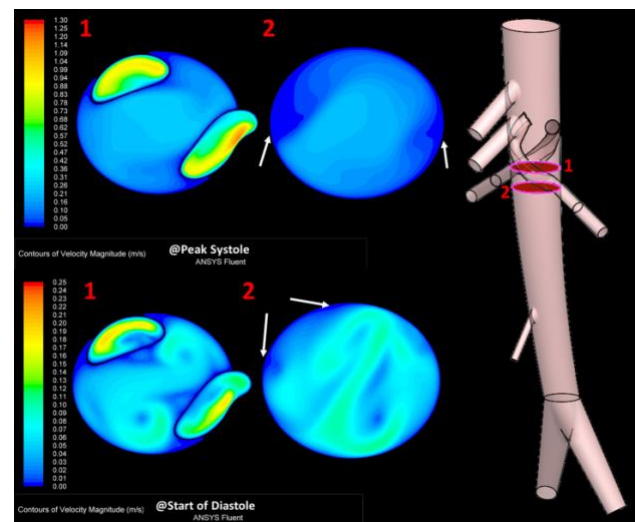
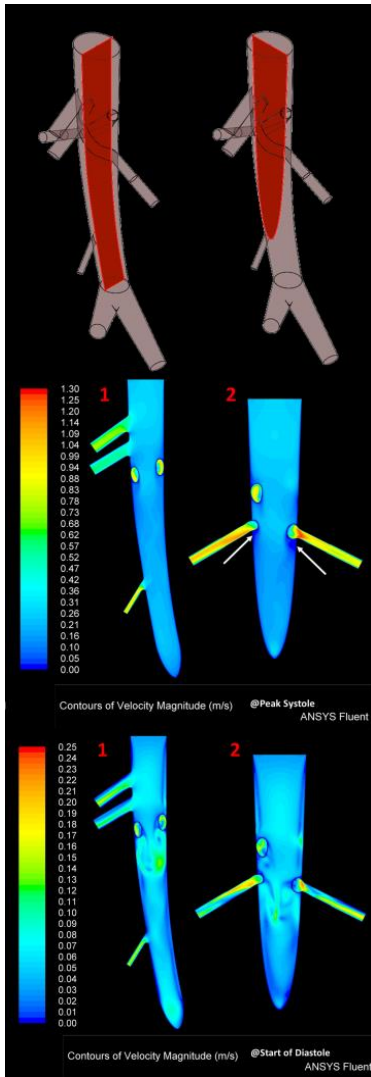
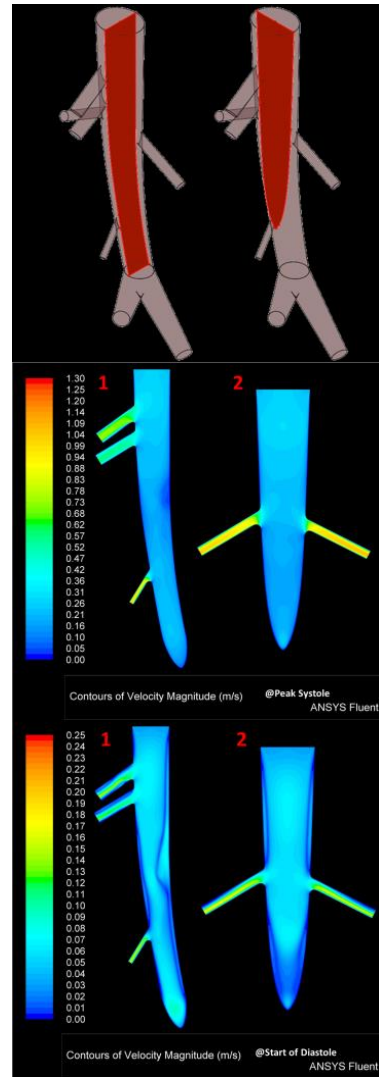


Figure 5: Velocity contours at peak systole and start of diastole at two distances below the CSGs (marked in red on the right). Arrows: stagnant regions.



**Figure 6:** Post ChEVAR abdominal aorta. Top: planes of velocity contours are marked in red. Middle: Velocity contours at peak systole. Bottom: Velocity contours at diastole beginning.



**Figure 8:** Healthy aorta. Top: planes of velocity contours are marked in red. Middle: Velocity contours at peak systole. Bottom: Velocity contours at diastole beginning.

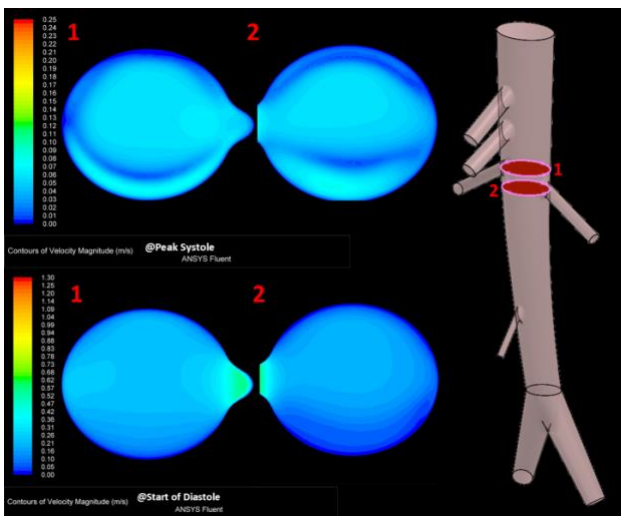


**Figure 7:** Velocity contours at peak systole and start of diastole at the same distances from the inlet as in Figure 5 (marked in red on the right) for a healthy aorta.

### 3.3 Flow Regime

Y (axial) component of the WSSs for the aorta post ChEVAR at various positions and distances from the inlet (according to Figures 9 and 10) are plotted in Figure 11 through Figure 13. Y component of the velocity along the centerline is plotted in Figure 14. The WSSs and the velocity follow the inlet velocity waveform. There are no high frequency components present. If the inlet blood flow waveform is free of high frequency components yet points inside the control volume present velocity/WSS waveforms with high frequency noise then the flow exhibits transitional regime behavior. If the waveforms are free of high frequency components/noise, it indicates a laminar flow regime (Bozzetto *et al*, 2015). This implies that the flow in the post ChEVAR abdominal aorta is free of transitional behavior and is indeed laminar.

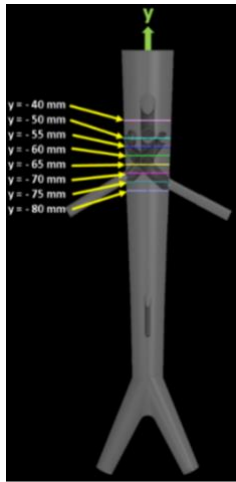


**Figure 9:** Section planes and their distances from the inlet.

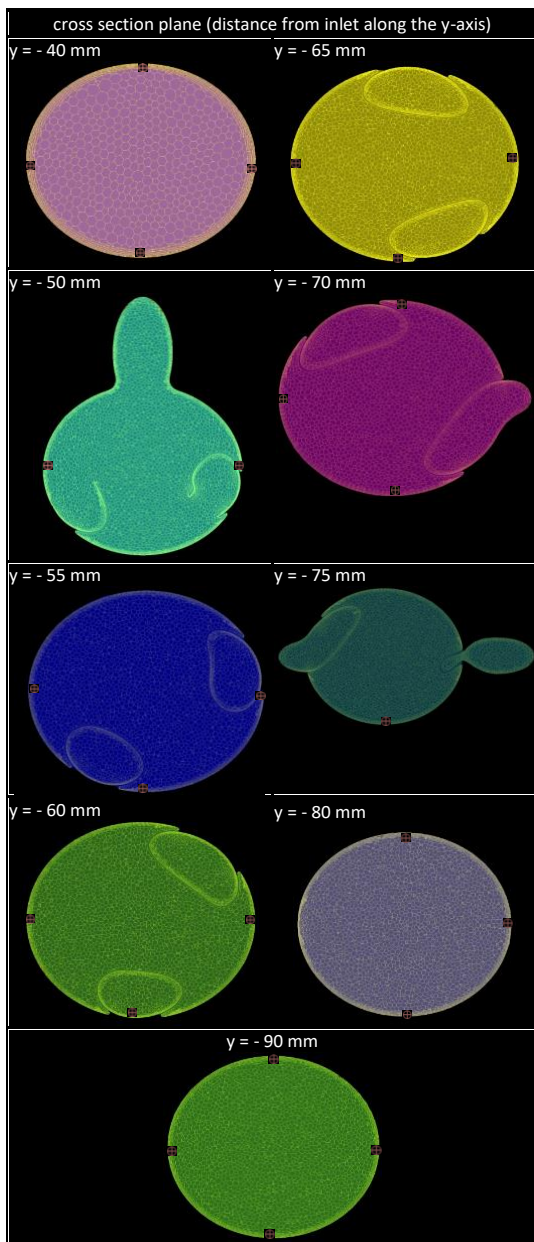


**Figure 10:** Points evaluated for WSSs at different horizontal planes.

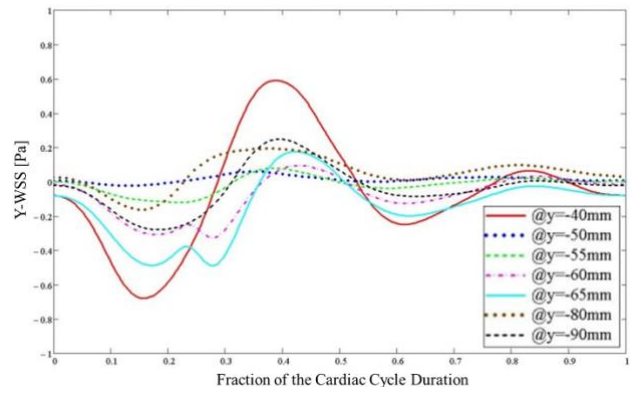


**Figure 11:** Y/axial component of WSS along the right side of the post ChEVAR aorta during the cardiac cycle.

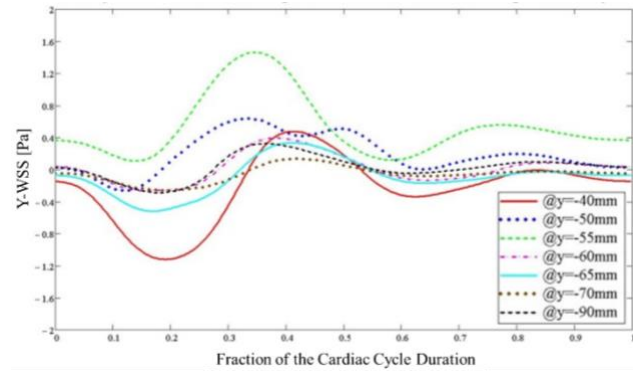


**Figure 12:** Y/axial component of WSS along the left side of the post ChEVAR aorta during the cardiac cycle.

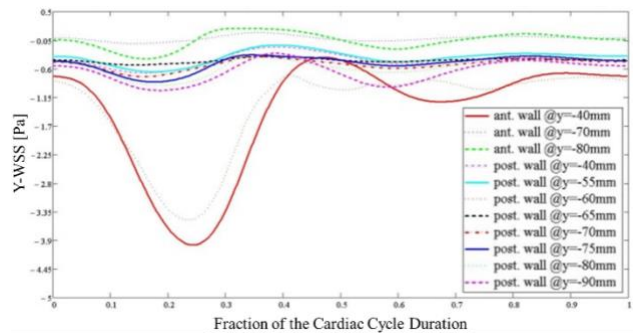


**Figure 13:** Y/axial component of WSS along the anterior and posterior of the post ChEVAR aorta during the cardiac cycle.

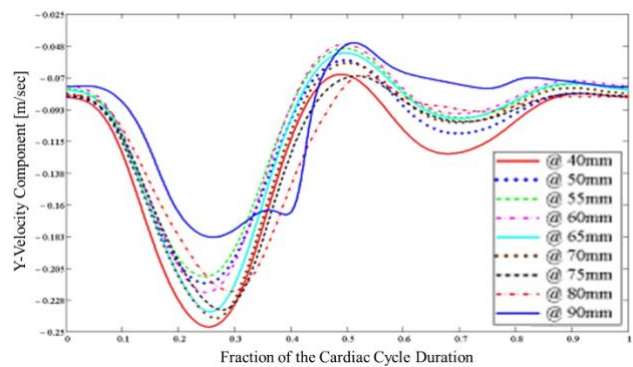


**Figure 14:** Y/axial component of velocity along the centerline of the post ChEVAR aorta.

## 4 Discussion and Conclusions

Our results suggest that CSGs presence in the abdominal aorta introduces variations in blood flow patterns and the formation of stagnant regions downstream from the CSGs throughout the cardiac cycle, potentially contributing to thrombosis (Ku *et al.*, 1997). However, as can be deduced from the smooth and non-disturbed nature of the curves portrayed in Figure 11 through Figure 14 and in accordance with a previous study, the CSGs do not cause the flow regime to become turbulent or transitional (Bozzetto *et al.*, 2015). This indicates limited flow field changes due to CSGs, thus further supporting the predictability of the flow in the abdominal aorta following an implantation of two renal stent grafts. These findings reconcile with data indicating a relatively high success rate in ChEVAR procedures performed in recent years, evident both in short and long-term patient follow ups (Zhang *et al.*, 2015).

## References

- M. Bozzetto, B. Ene-Iordache, and A. Remuzzi. Transitional Flow in the Venous Side of Patient-Specific Arteriovenous Fistulae for Hemodialysis. *Ann. Biomed. Eng.*, pp. 1–14, 2015. doi: 10.1007/s10439-015-1525-y.
- R. Coscas, H. Kobeiter, P. Desgranges, and J.-P. Becquemin. Technical aspects, current indications, and results of chimney grafts for juxtarenal aortic aneurysms. *J. Vasc. Surg.*, 53(6):1520–7, 2011. doi.org/10.1016/j.jvs.2011.01.067.
- J. L. de Bruin, K. K. Yeung, W. W. Niepoth, R. J. Lely, Q. Cheung, A. de Vries, and J. D. Blankensteijn. Geometric study of various chimney graft configurations in an in vitro juxtarenal aneurysm model. *J. Endovasc. Ther.*, 20(2): 184–90, 2013. doi.org/10.1583/1545-1550-20.2.184.
- B. Ene-Iordache, L. Mosconi, G. Remuzzi, and A. Remuzzi. Computational fluid dynamics of a vascular access case for hemodialysis. *J. Biomech. Eng.*, 123(3): 284–292, 2001. doi: 10.1115/1.1372702.
- M. H. Friedman, C. B. Barger, D. D. Duncan, G. M. Hutchins and F. F. Mark. Effects of Arterial Compliance and Non-Newtonian Rheology on Correlations Between Intimal Thickness and Wall Shear. *J. Biomech. Eng.*, 114(3): 317, 1992. doi:10.1115/1.2891389.
- D. N. Ku. Blood Flow in Arteries, *Annu. Rev. Fluid Mech.*, 29: 399–434, 1997. doi.org/10.1146/annurev.fluid.29.1.399.
- D.-C. Guo, C. L. Papke, R. He, and D. M. Milewicz. Pathogenesis of thoracic and abdominal aortic aneurysms. *Ann. N. Y. Acad. Sci.*, 1085: 339–52, 2006. doi: 10.1196/annals.1383.013.
- H. Kandail, M. Hamady, and X. Y. Xu. Patient-specific analysis of displacement forces acting on fenestrated stent grafts for endovascular aneurysm repair. *J. Biomech.*, 47(14): 3546–3554, 2014.
- J. E. Moore, D. N. Ku, C. K. Zarins and S. Glagov. Pulsatile flow visualization in the abdominal aorta under differing physiologic conditions: implications for increased susceptibility to atherosclerosis. *J. Biomech. Eng.*, 114: 391–397, 1992. doi:10.1115/1.2891400.
- J. E. Moore, S. Glagov, and D. N. Ku. Fluid wall shear stress measurements in a model of the human abdominal aorta: oscillatory behavior and relationship to atherosclerosis. *Atherosclerosis*, 9150: 225–240, 1994. doi.org/10.1016/0021-9150(94)90207-0.
- L. Morris, P. Delassus, M. Walsh, and T. McGloughlin. A mathematical model to predict the in vivo pulsatile drag forces acting on bifurcated stent grafts used in endovascular treatment of abdominal aortic aneurysms (AAA). *J. Biomech.*, 37(7): 1087–95, 2004. doi.org/10.1016/j.jbiomech.2003.11.014.
- T. Shipkowitz, V. G. J. Rodgers, L. J. Frazin, and K. B. Chandran. Numerical study on the effect of steady axial flow development in the human aorta on local shear stresses in abdominal aortic branches. *J. Biomech.*, 31: 995–1007, 1998.
- C. A. Taylor, T. J. R. Hughes, and C. K. Zarins. Finite Element Modeling of Three-Dimensional Pulsatile Flow in the Abdominal Aorta: Relevance to Atherosclerosis. *Ann. Biomed. Eng.*, 26: 975–987, 1998.
- Y. Li, T. Zhang, W. Guo, C. Duan, R. Wei, Y. Ge, X. Jia, and X. Liu. Endovascular chimney technique for juxtarenal abdominal aortic aneurysm: a systematic review using pooled analysis and meta-analysis. *Ann. Vasc. Surg.*, 29(6): 1141–50, 2015. doi.org/10.1016/j.avsg.2015.02.015.